Talanta 113 (2013) 1–6

Contents lists available at SciVerse ScienceDirect

Talanta

journal homepage: www.elsevier.com/locate/talanta

A sensitive NADH and ethanol biosensor based on graphene–Au nanorods nanocomposites

Li Li [a], Hongmei Lu [a,b,*], Liu Deng [a,b,*]

[a] College of Chemistry and Chemical Engineering, Central South University, Changsha 410083, PR China
[b] Key Laboratory of Resources Chemistry of Nonferrous Metals, Ministry of Education, Central South University, Changsha 410083, PR China

ARTICLE INFO

Article history:
Received 21 January 2013
Received in revised form
21 March 2013
Accepted 28 March 2013
Available online 6 April 2013

Keywords:
Graphene
Au nanorods
NADH
Ethanol biosensor

ABSTRACT

In this paper, a simple strategy for the synthesis of graphene–Au nanorods hybrid nanosheets (GN–AuNRs) through electrostatic interaction has been demonstrated. Due to the synergistic effect between AuNRs and GN, the hybrid nanosheets exhibited excellent performance toward dihydronicotinamide adenine dinucleotide (NADH) oxidation, with a low detection limit of 6 μM. The linear GN–AuNRs also served as a biocompatible and electroactive matrix for enzyme assembly to facilitate the electron transfer between the enzyme and the electrode. Using alcohol dehydrogenase (ADH) as a model system, a simple and effective sensing platform was developed for ethanol assay. The response displayed a good linear range from 5 to 377 μM with detection limit 1.5 μM. Furthermore, the interference effects of redox active substances, such as uric acid, ascorbic acid and glucose for the proposed biosensor were negligible.

1. Introduction

Dihydronicotinamide adenine dinucleotide (NADH) is a significant coenzyme related to the redox reactions of cellular respiration. There are about 300 dehydrogenases performing their biocatalytic function which depends on the converting process of $NADH/NAD^+$ [1]. Therefore researches on the electrochemical oxidation of NADH, and the fabrication of NAD^+-dependent enzymatic biosensors have drawn considerable attention [2–5]. However, direct oxidation of NADH at bare electrode occurs at high overpotential (0.6–0.8 V) and suffers from low sensitivity and the fouling of the electrode surface by its oxidation products [6,7], which cause loss of selectivity, reproducibility and stability. In recent years, many nanomaterials, such as poly(1,2-diaminobenzene) nanotubules, TiO_2 nanostructured films, carbon nanotubes (CNTs), carbon nanofibers (CNFs) and gold nanoparticles (AuNPs), have been devoted to decrease the high overpotential for NADH electro-oxidation and minimize the surface fouling [8–13].

Graphene, a two-dimensional and single layer sheet of sp^2 hybridized carbon atoms, has attracted a great deal of attention from both the experimental and theoretical scientific communities in the past several years [14]. Due to its exceptional electron transfer property and large surface-to-volume ratio, graphene has been used as an electrochemical biosensors platform [15–17]. Gold nanomaterials offer a substantial increase of available surface area and a biocompatible platform for functionalization in biosensing or therapeutic applications [18–20]. Gold nanorods, anisotropic and elongated nanoparticles, are of good biocompatibility, simple preparation and high stability, which have been widely used as the immobilization matrix for electrochemical biosensors [21,22] and bioelectrocatalysis [23,24]. In addition, the surface chemistry of AuNRs is versatile, allowing the linking of various biofunctional groups, like amphiphilic polymers, sugars, nucleic acids and proteins, through strong Au–S or Au–N bonding or through physical adsorption [25,26]. Therefore, AuNRs can improve adhering ability of the composite film on electrode surface and provide an ideal matrix for enzyme immobilization and biosensor fabrication [23,27]. If we can obtain the AuNRs–graphene hybrid nanosheets, it will provide excellent opportunities for applications in the fields of enzyme biosensors, electrocatalysis, electronics, etc.

In the present paper, we reported a NADH and ethanol biosensor based on the hybrid graphene–gold nanorods nanocomposite (GN–AuNRs), which was synthesized by a simple electrostatic self-assemble process. The GN–AuNRs modified electrode showed good electrocatalytic activity to the NADH oxidation. GN–AuNRs could provide a suitable microenvironment to retain the enzyme activity and facilitate the electron transfer process of the enzymatic reaction. ADH was used as a model enzyme that could be simply immobilized on the electrode surface by adsorption process. The GN–AuNRs–ADH exhibited excellent amperometric response to ethanol, holding great promise to fabricate biosensors for practical applications.

* Corresponding authors. Tel.: +86 731 88836376; fax: +86 731 88879616.
E-mail addresses: Hongmeilu@csu.edu.cn (H. Lu), Dengliu_erita@yahoo.com.cn (L. Deng).

0039-9140/$ - see front matter © 2013 Elsevier B.V. All rights reserved.
http://dx.doi.org/10.1016/j.talanta.2013.03.074

2. Experimental

2.1. Reagents

Flake graphite (500 mesh, 25 μm) was obtained from Sinopharm Chemical Reagent Co., Ltd. (China). Chloroauric acid ($HAuCl_4 \cdot 3H_2O$), sodium borohydride ($NaBH_4$), hexadecyl trimethyl ammonium bromide (CTAB), ascorbic acid (AA), uric acid (UA), silver nitrate ($AgNO_3$), polyvinylpyrrolidone (PVP), nicotinamide adenine dinucleotide (NADH), and ADH (E.C. 1.1.1.1, 340 U mg^{-1}, from *Saccharomyces cerevisiae*) were all purchased from Sigma-Aldrich. The other reagents were of analytical grade and used without further purification. Phosphate buffered saline (PBS, 0.1 M, pH 7.0) was used as the supporting electrolyte. All solutions were prepared with double-distilled water.

2.2. Instruments

The morphologies of GN–AuNRs, GN and AuNRs were observed on a transmission electron microscope (TEM, Tecnai G220 S-Twin), operating at an accelerating voltage of 200 KV. The UV–vis spectra were obtained by a Shimadzu 1800 UV–vis spectrophotometer. All electrochemical measurements were carried out on a CHI 660 electrochemical workstation (Shanghai CH Instruments, China) with a conventional three-electrode system consisting of glassy carbon electrode (GCE) as working electrode, platinum wire as auxiliary electrode, and Ag/AgCl (saturated KCl) as reference electrode. Zeta potential was acquired by zetasizer nanoseries (ZEN 3600).

2.3. Preparation of PVP-protected GN

Graphene oxide (GO) was prepared by oxidizing natural graphite powder using a modified Hummers and Offeman's method [28]. The PVP-protected GN was prepared as the following: 2 mg GO was dispersed in 4 mL distilled water by ultrasonication for 2 h. After that, 30 μL concentrated ammonia and 4 mg mL^{-1} PVP aqueous solution (4 mL) were added into the above GO dispersions under stirring. Five minutes later, 20 μL hydrazine solution was added into the above mixed solution. Then the resulting solution was put into 60 °C water bath for 3.5 h. After the obtained black dispersion was centrifuged, the PVP-protected GN nanosheets were acquired and re-dispersed into 4 mL water under ultrasonication.

2.4. Preparation of AuNRs

Gold nanorods were prepared according to the seed-mediated growth method optimized by Nikoobakht and El-Sayed [29]. Briefly, a seed solution was prepared by mixing 5 mL of hexadecyl trimethyl ammonium bromide (CTAB, 0.2 M) and 5 mL of chloroauric acid ($HAuCl_4$, 0.5 mM) with 0.6 mL of freshly prepared 10 mM ice-cold sodium borohydride ($NaBH_4$) solution. The color of the solution changed from dark yellow to brownish yellow under vigorous stirring, indicating the formation of the seed solution. For the synthesis of gold nanorods, 1.5 mL of 4 mM silver nitrate ($AgNO_3$) aqueous solution was mixed with 50 mL of 1.0 mM $HAuCl_4$, and the mixed solution was added to 50 mL of 0.2 M CTAB solution. After gentle mixing of the solution, 0.70 mL of 0.1 M ascorbic acid (AA) was added. While this mixture was continuously stirred, 120 μL of the seed solution was added finally to initiate the growth of the gold nanorods. Gold nanorods with an aspect ratio of 3.5 ± 0.4 were yielded. These gold nanorods were aged for 20 h to ensure full growth. Finally, the gold nanorods were centrifuged three times and re-dispersed in water.

2.5. Preparation of GN–AuNRs nanocomposite

1 mL colloid AuNRs were added to 1 mL PVP–GN (0.05 mg mL^{-1}) under stirring and sonication. After 2 h, the resulting GN–AuNRs nanocomposite was collected by centrifugation, and re-dispersed in water to form a homogenous dispersion of GN–AuNRs with ultrasonication.

2.6. Preparation of modified electrodes

The glassy carbon electrodes (GCEs) (4 mm in diameter) were polished with 0.3 μm alumina slurry followed by rinsing with double distilled water, ethanol and double distilled water, subsequently. The modified electrodes were completed by casting 10 μL of the GN–AuNRs on the surface of the electrode and dried for 2 h at room temperature in a desiccator. The GN–AuNRs–ADH modified electrode was prepared by casting 10 μL of 1 mg mL^{-1} GN–AuNRs solution containing 10 mg mL^{-1} ADH and allowed to dry at 4 °C overnight.

3. Result and discussion

3.1. The characterization of GN–AuNRs hybrid nanosheets formation

Non-protected graphene sheets tended to form agglomerates irreversibly due to intermolecular strong π–π stacking and van der Waals interaction. The GN aggregated into clusters in a short time when AuNRs were directly added into pure GN solution. Therefore PVP was used as the dispersant and stabilizer to overcome aggregation of graphene sheets. After PVP introduction, the GN–AuNRs had excellent solubility in water. Fig. 1 shows typical transmission electron microscopy (TEM) images of the synthesized GN, AuNRs and GN–AuNRs. TEM image of the GN sheets clearly shows an ultra-thin paper with wrinkled morphology. The TEM

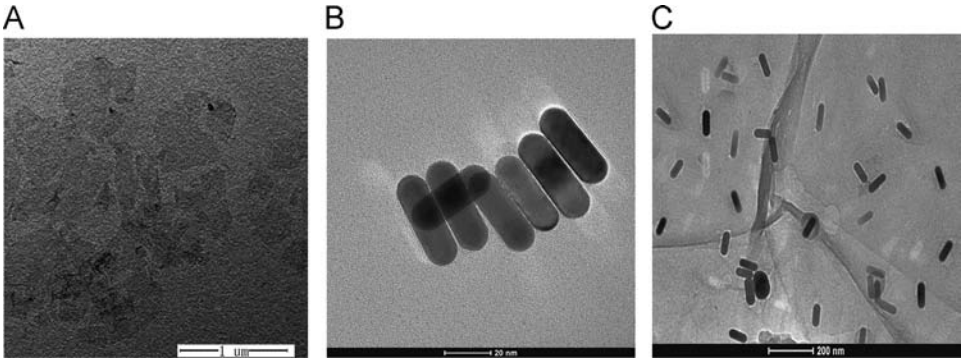

Fig. 1. TEM of (A) GN, (B) AuNRs and (C) GN–AuNRs.

image of the as-prepared gold nanorods exhibits nanorods ~40 nm in length. Each nanorod with aspect ratio 3.5 ± 0.4 has a smooth surface. The surface charge (zeta potential) of PVP-protected GN was −30.0 mV, which suggested that the GN was highly negatively charged when wrapped by negatively charged PVP. The surface charge of AuNRs was +23.0 mV, which indicated that the AuNRs were positively charged. Thus, the GN could act as an electrostatic anchor for absorption of positively charged AuNRs through the self-assemble methodology. The assembly of AuNRs on the GN surface was confirmed by the TEM images (Fig. 1C). UV–vis absorption spectrum was used to investigate the interaction between the AuNRs and the GN. As shown in Fig. 2, the GN dispersion displays a maximum absorption at 263 nm which is due to the π–π^* transition of aromatic C=C bonds and a shoulder at 270–280 nm which corresponds to the n–π^* transition of the C–O bond. The immobilization of AuNRs on the graphene sheets surface could be readily monitored by UV–vis spectrophotometry. Before AuNRs anchored in GN, the AuNRs solution with light red-brown color displayed two characteristic surface plasmon absorption peaks at 511 and 700 nm. After AuNRs anchored in GN, a color change occurred from red-brown color to blue-black. The transverse plasmon absorption bands shifted to the blue slightly, while the longitudinal plasmon absorption bands remained at the same place with the intensity decrease. The new peak exhibited at 263 nm could be ascribed to GN in the GN–AuNRs. This indicated that the electrostatic force between GN and AuNRs allowed the successful deposition of AuNRs on GN surface.

3.2. Detection of NADH at the GN–AuNRs modified electrodes

As shown in Fig. 3, curves *b* and *a* are cyclic voltammograms (CVs) of the GN–AuNRs modified GC electrode in PBS (pH 7.0) with and without NADH, respectively. When NADH was absent, there was no electrocatalytic oxidation peak. However, in the presence of NADH, a remarkable catalytic oxidation current at the modified electrode occurred at ca. 30 mV, which negatively shifted 570 mV, compared with that at the bare GCE (ca. 600 mV). The electrocatalytic current increased significantly with a further increase of the concentration of NADH. The electrochemical results demonstrated that the GN–AuNRs composite modified electrode maintained a good electrochemical activity of NADH and could be applied to the field of electrochemistry.

A detailed study of the electrocatalytic behavior toward NADH oxidation on the GN–AuNRs/GC electrode was also carried out in this section. To discern the contribution of individual components and the possible synergistic effect among them, control

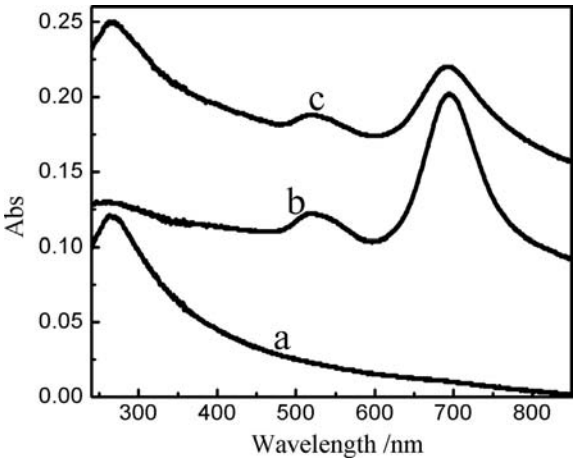

Fig. 2. UV–vis spectra of (a) GN, (b) AuNRs and (c) GN–AuNRs.

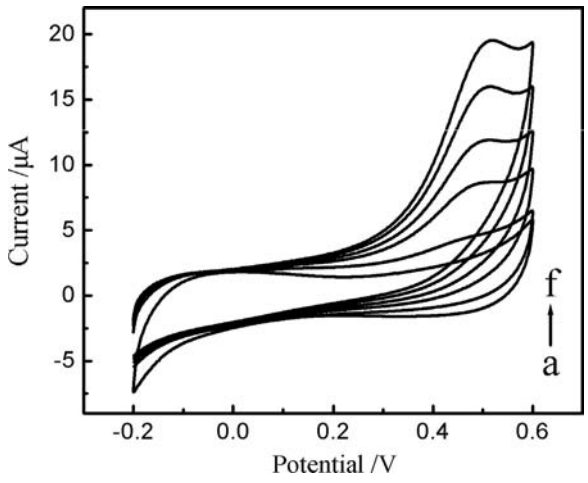

Fig. 3. CVs of GN–AuNRs/GC electrode in the presence of (a) 0, (b) 1, (c) 2, (d) 3, (e) 4, and (f) 5 mM NADH in 0.1 M PBS (pH 7.0); scan rate: 50 mV s^{-1}.

experiments on GN/GC and AuNRs/GC electrodes were carried out. As shown by the cyclic voltammograms in Fig. 4A, the electrochemical oxidation of NADH on the AuNRs/GC electrode starts at 0.2 V, which is a slight negative shift of the onset potential for the NADH oxidation on the bare GC electrode. At the same time, the GN modified electrode shows much better electrocatalytic activity. As shown in Fig. 4B, the electrochemical oxidation of NADH already starts at 0.1 V, indicating that graphene is a good candidate for accelerating electron transfer for the NADH oxidation. This result was in good agreement with those observed previously [30–32]. When AuNRs were incorporated in the GN–AuNRs/GC electrode, the anodic current nearly three times as high as that of the GN/GC electrode was observed, and the onset potential has a slight negative shift to 30 mV. The onset potential for NADH oxidation on this GN–AuNRs/GC electrode appeared as the most negative value amongst all of these electrodes, as presented in Fig. 3. These results demonstrated that the GN–AuNRs/GC electrode exhibited the best response toward electrochemical oxidation of NADH. The increased anodic current on the GN–AuNRs composite film electrode should be due to the synergistic effects between the GN nanosheets and AuNRs because the current $I_{(GN-AuNRs)} > (I_{GN}+I_{AuNRs})$, where $I_{(GN-AuNRs)}$ is the current due to the oxidation of NADH at the GN–AuNRs/GC electrode, and I_{GN} and I_{AuNRs} are the oxidation currents of NADH at GN and AuNRs-modified GC electrodes, respectively. Such synergy has been recently observed by several studies of the electrocatalytical small biomolecules on the CNTs and nanomaterials integrated system [33–35]. In the NADH biosensor on the basis of GN–AuNRs nanocomposite, graphene with a large surface-to-volume ratio and high efficiency of electron transfer provided the necessary conduction pathways and allowed efficient electron tunneling, which facilitated electrical communication between NADH and the electrode surface. Due to the well-distributed dispersion of electron conductor AuNRs in sensing film and the formation of three-dimensional electronic conductive network by the close contact between graphene and AuNRs, the electron transfer in film was accelerated, which led to the increase of oxidation of NADH on the electrode surface. At the same time, these adsorbed AuNRs could be more effective to offer electron transfer path, and played a role of the nanomicro-electrodes to accelerate electron transfer between the electrode and the analyte.

Fig. 5A exhibits an amperometric response to the successive addition of NADH in 0.1 M PBS (pH 7.0) at the GN–AuNRs nanocomposite film modified electrode. The response time was within 10 s, indicating a fast process and well catalytic oxidation of

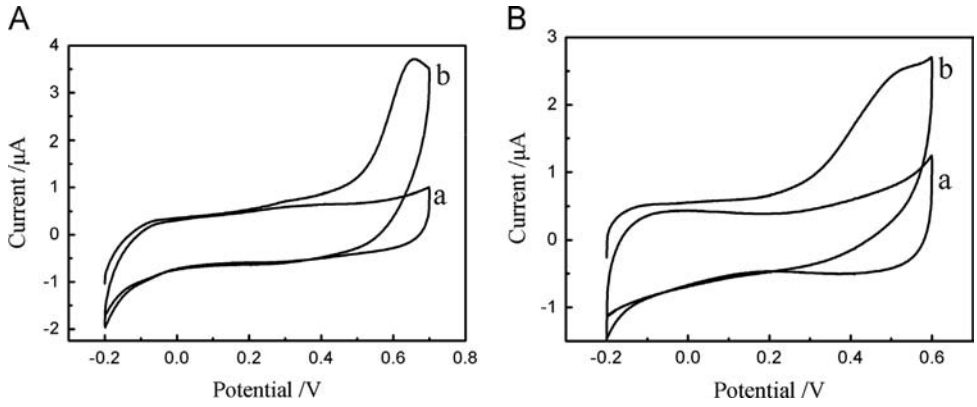

Fig. 4. CVs of (A) AuNRs/GC electrode and (B) GN/GC electrode in the presence of (a) 0 and (b) 2 mM NADH in 0.1 M PBS (pH 7.0); scan rate: 50 mV s^{-1}.

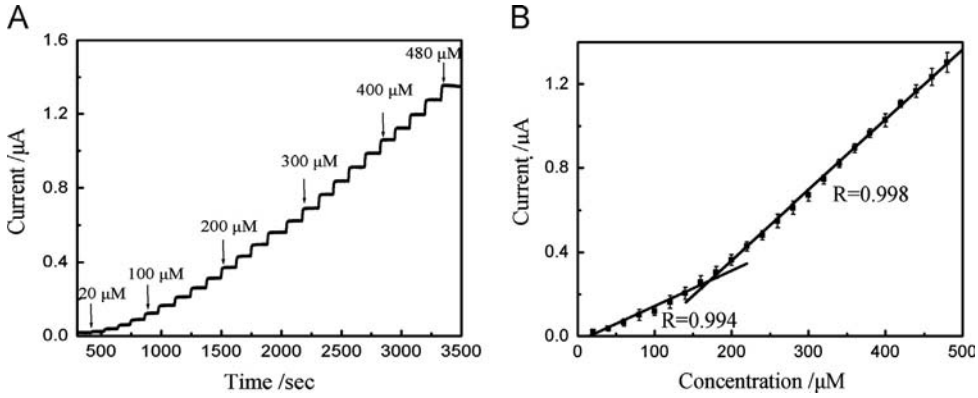

Fig. 5. (A) Amperometric response of GN–AuNRs/GC electrode for the oxidation of NADH at +0.4 V in 0.1 M PBS (pH 7.0). Each addition increases the concentration of NADH by 20 μM. (B) The calibration plot of the concentration of NADH with current at GN–AuNRs/GC electrode. Standard deviation was obtained from three different electrodes.

NADH by GN–AuNRs nanocomposite. The response displayed two linear concentration ranges (Fig. 5B); one from 20 to 160 μM with a correlation coefficient of 0.994 and sensitivity of 10.27 μA mM^{-1} cm^{-2} and another from 160 to 480 μM with a correlation coefficient of 0.998 and sensitivity of 27.07 μA mM^{-1} cm^{-2}. The detection limit was 6 μM based on signal to noise ratio of 3. The linear response range was wider than that of 25–250 μM reported previously with a graphene-CNTs-based NADH amperometric sensor [36] and that of 10–240 μM with a NADH sensor based on Au–TiO_2/graphene nanocomposite film [37]. The obtained detection limit was lower than that of 20 μM reported at graphene sheets modified electrode [38] and that of 18 μM based on neutral red functionalized carbon nanotube/plasma-polymerized film composite modified electrode [39].

The GN–AuNRs/GC electrode also exhibited an excellent stability of amperometric NADH response. The voltammetric response of the GN–AuNRs nanocomposite modified electrode being left in 20 mM NADH solution for 30 min decreased 0.3% (Fig. 6). This demonstrated a resistance of the GN–AuNRs nanocomposite modified electrode to fouling, which was commonly met at other solid electrodes for oxidation of NADH. The good operational stability of the GN–AuNRs nanocomposite modified electrode was due to faster charge transfer and lower overpotential for the oxidation of NADH. The improved kinetics of electron transfer limited the amount of radical intermediates and their dimerization, which typically caused fouling of the electrode surface during the oxidation of NADH via two successive one-electron-transfer steps. Repetitive amperometric measurements for 2 mM NADH at the GN–AuNRs nanocomposite electrode gave a relative standard deviation (RSD) of 3.7% ($n=10$). This good repeatability should be related to the GN–AuNRs capability to minimize the electrode surface fouling after NADH oxidation.

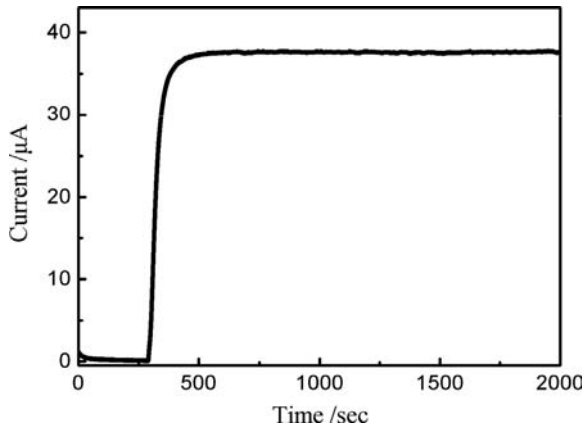

Fig. 6. Stability of current response of 20 mM NADH at GN–AuNRs/GC electrode at applied potential of +0.4 V in 0.1 M PBS (pH 7.0).

3.3. GN–AuNRs–ADH-based biosensor for ethanol

Because of the excellent electrocatalytic activity of the GN–AuNRs nanocomposite modified electrode toward the oxidation of NADH, an amperometric ethanol biosensor was fabricated by incorporating a model enzyme ADH into the GN–AuNRs nanocomposite film. The excellent electric property and incompact open structure of GN–AuNRs film could facilitate the access of a substrate and cofactor NAD^+ to the ADH and result in good catalytic behavior to the substrate. The amount of enzyme immobilized within the biocomposite matrix was crucial for the ethanol biosensor sensitivity. The amperometric responses were examined

as a function of the ADH (1, 5, 10 and 15 mg mL^{-1}) loading within the GN–AuNRs–ADH biocomposite. The ethanol biosensor responses enhanced by increasing the immersed time from 1 mg mL^{-1} to 10 mg mL^{-1}. The increase was accounted for more enzymatic redox active sites in the GN–AuNRs–ADH biocomposite. The response of the biosensor reduced after higher ADH loading. The abundant ADH within GN–AuNRs–ADH biocomposite disturbed the electron relaying capacity of the GN–AuNRs nanostructure due to the insulting ADH. As a result, 10 mg mL^{-1} ADH was chosen as the optimum enzyme modification for the following biosensor fabrication. The effect of the concentration of NAD^+ on the biosensor response was investigated with a constant amount of enzyme loading and ethanol concentration. The catalytic current for ethanol increased with increasing concentration of NAD^+ and reached a maximum value at around 30 mM. A further increase in the concentration of NAD^+ resulted in a decrease in the catalytic current, probably due to the inhibitory effect of NAD^+. Because the enzyme activity was dependent on the pH value of a buffer solution, the effect of pH value on the current response was examined. The current response increased by increasing the pH value in the range of 6.0–7.0, and reached a maximum value at pH 7.0. It decreased dramatically at pH above 7.0, which was attributed to the unstability of NAD^+ in alkaline solution [40]. Therefore, a solution of pH 7.0 and 30 mM NAD^+ in 0.1 M PBS were selected.

Fig. 7 shows CV response at GN–AuNRs–ADH/GC electrode toward ethanol. GN–AuNRs–ADH biocomposite modified GCE exhibited an excellent electrocatalytic activity toward ethanol. In the presence of ethanol, a remarkable catalytic oxidation current at the modified electrode occurred at ca. 35 mV, which would facilitate low-potential amperometric measurement of ethanol. Fig. 8A exhibits the steady-state response to the successive addition of ethanol at GN–AuNRs–ADH/GC electrode. The response of the sensor was fast, and the response time was ca. 10 s. The anodic current increased linearly with ethanol concentration over the range from 5 to 377 μM (Fig. 8B), with a good sensitivity of 102 μA mM^{-1} cm^{-2}. The limit of detection was estimated at a signal-to-noise ratio of 3 to be 1.5 μM, which was much lower than that of 24 μM and 2.85 mM reported for sensors based on multiwalled carbon nanotubes [41] and a Clark-type transducer [42], respectively. The RSD, estimated from the slopes of the calibration plots of six different and freshly prepared ethanol sensors, was 4.6%, indicating good fabrication reproducibility. The sensors could be repeatedly used for ethanol monitoring. The assay precision of the sensors was examined at an ethanol concentration of 100 μM. The RSD for six determinations was 5.1%. The examination of the batch-to-batch reproducibility showed a RSD of 7.2% for the slopes of calibration plots of six sensors made at the same electrode independently. In real samples, there were some coexisting electroactive species such as methanol (MeOH), 1-propanol (1-Prop), 1-butanol (1-But), uric acid (UA), ascorbic acid (AA) and glucose (GL) that might affect the biosensor response. The selectivity and anti-interference advantages of the biosensor were demonstrated (Fig. 9). A well-defined ethanol response was observed at the biosensor, whereas MeOH, 1-Prop, 1-But, GL, AA, UA resulted in negligible signals. Therefore, highly selective response to ethanol was obtained without the use of a perm-selective membrane or enzymatic preoxidation. These results demonstrated that this biosensor had good selectivity, stability and reproducibility, as required for the determination of ethanol.

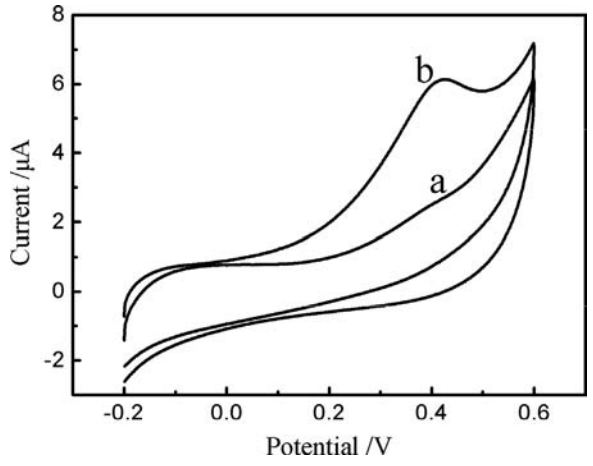

Fig. 7. CVs of GN–AuNRs–ADH/GC electrode in the presence of (a) 0 and (b) 5 mM ethanol in 0.1 M PBS (pH 7.0); scan rate: 50 mV s^{-1}.

3.4. Determination of ethanol in alcoholic beverage samples

To illustrate feasibility of the fabricated ethanol biosensor in practical analysis, the GN–AuNRs–ADH/GC electrode was used to detect ethanol in three different alcoholic beverages: beer, red wine and white spirit. These alcoholic beverages were bought from the local supermarket. Then the samples were assayed with the biosensor rapid and stable amperometric responses were acquired when the sample was added into test system. The contents of ethanol could be calculated from the calibration curve. The obtained results are listed in Table 1, which indicated that the determination of ethanol using GN–AuNRs–ADH coated on GC was effective and sensitive.

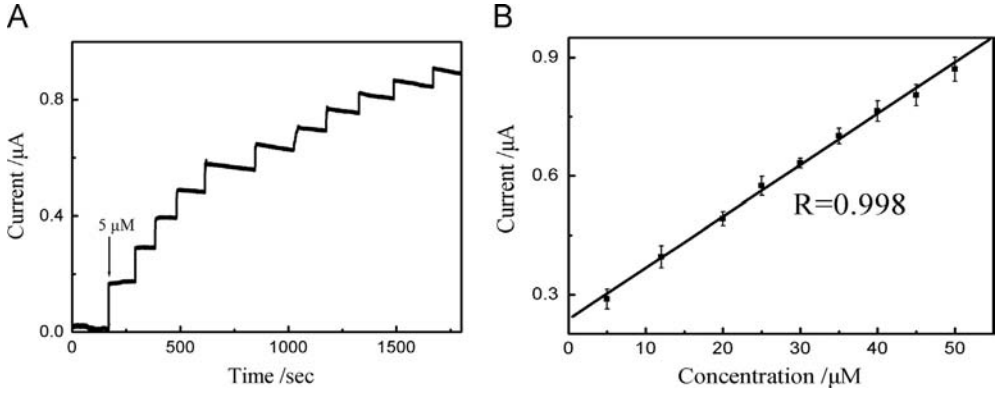

Fig. 8. (A) Amperometric response of GN–AuNRs–ADH/GC electrode with successive addition of ethanol in stirred 0.1 M PBS (pH 7.0) solution containing 30 mM NAD^+. (B) The calibration plot of the concentration of ethanol with current at GN–AuNRs–ADH/GC electrode. Standard deviation was obtained from three different electrodes.

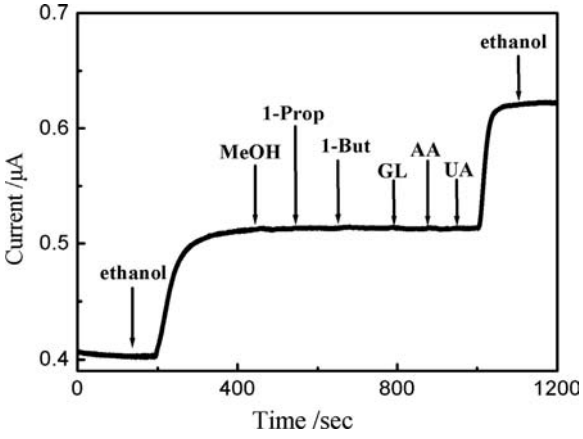

Fig. 9. Amperometric response of the GN–AuNRs–ADH/GC electrode to ethanol (0.1 mM), MeOH (1 mM), 1-Prop (1 mM), 1-But (1 mM), UA (1 mM), AA (1 mM) and GL (1 mM) in 0.1 M PBS (pH 7.0) containing 30 mM NAD^+.

Table 1
Determination of ethanol in real samples with GN–AuNRs–ADH/GC electrode.

Sample	Found (M)[a]	Commercial (M)	RSD (%)
Beer	1.01	0.95	4.32
Red wine	2.13	1.97	5.51
White spirit	10.80	11.50	4.43

[a] Average of three measurements.

4. Conclusions

A one-step, wet-chemical strategy for the rapid preparation of graphene–gold nanorods hybrid nanosheets was demonstrated. The proposed method was unique in its simplicity. The resulting GN–AuNRs were used as advanced electrode materials and extensively investigated by various characterization methods, including TEM, UV and electrochemistry. The new composite material combined the unique and attractive electrocatalytic behavior of AuNRs and GN, and biocompatible properties of GN. On the basis of these unique properties of the new material, we developed a sensitive assay for ethanol detection. The biosensor exhibited a fast response, a broad linear range, a low detection limit with satisfactory stability and repeatability and would have great potential application in determination of ethanol. These desirable biosensor performances were attributed to the open architectures of the GN–AuNRs, the large surface area of GN for enzyme immobilization, fast mass transport due to the large interlayer distance of the hybrid nanosheets, high conductivity and good biocompatibility of GN, and the synergistic catalytic effect between GN and AuNRs. The fabrication method of the biosensor has many advantages such as ease of fabrication, enhanced electrocatalysis, efficiently preserving the activity of enzyme molecules, and effective discrimination to the common interfering species. GN–AuNRs nanocomposite, with favorable electrochemical activity, might pave the way in developing new solid support-enzyme nanohybrids for the fabrication of electrochemical sensing and bio-sensing applications.

Acknowledgment

We thank the National Natural Science Foundation of China for support of the projects (Nos. (20975115, 21105126 and 21175157), China Hunan Provincial Science and Technology Department for support of the project no. (2012FJ4139), Central South University for special support of the basic scientific research project (No. (2010QZZD007), China Postdoctoral Science Foundation for support of the project (Nos. (2011M500126, 2012T50656 and 201104511).

References

[1] H.C. Chang, X.J. Wu, C.Y. Wu, Y. Chen, H. Jiang, X.M. Wang, Analyst 136 (2011) 2735–2740.
[2] C.S. Shan, H.F. Yang, D.X. Han, Q.X. Zhang, A. Ivaska, L. Niu, Biosens. Bioelectron. 25 (2010) 1504–1508.
[3] M. Zhang, A. Smith, W. Gorski, Anal. Chem. 76 (2004) 5045–5050.
[4] B.K. Jena, C.R. Raj, Anal. Chem. 78 (2006) 6332–6339.
[5] M. Zhang, C. Mullens, W. Gorski, Anal Chem. 79 (2007) 2446–2450.
[6] R. Scipioni, M. Pumera, M. Boero, Y. Miyahara, T. Ohno, J. Phys. Chem. Lett. 1 (2009) 122–125.
[7] M. Pumera, R. Scipioni, H. Iwai, T. Ohno, Y. Miyahara, M. Boero, Chem. Eur. J. 15 (2009) 10851–10856.
[8] J. Zhu, X. Chen, W.S. Yang, Sens. Actuators B: Chem. 150 (2010) 564–568.
[9] Q. Wang, H. Tang, Q.J. Xie, L. Tan, Y.Y. Zhang, B.M. Liet al., Electrochim. Acta 52 (2007) 6630–6637.
[10] Y. Fan, X. Yang, C.P. Yang, J.H. Liu, Electroanalysis 24 (2012) 1334–1339.
[11] L.N. Pelster, M.T. Meredith, S.D. Minteer, Electroanalysis 24 (2012) 1011–1018.
[12] H. Teymourian, A. Salimi, R. Hallaj, Biosens. Bioelectron. 33 (2012) 60–68.
[13] H. Teymourian, A. Salimi, R. Hallaj, Talanta 90 (2012) 91–98.
[14] S. Stankovich, D.A. Dikin, G.H.B. Dommett, K.M. Kohlhaas, E.J. Zimney, E. A. Stachet al., Nature 442 (2006) 282–286.
[15] D.R. Kauffman, A. Star, Analyst 135 (2010) 2790–2797.
[16] M. Pumera, Chem. Soc. Rev. 39 (2010) 4146–4157.
[17] W. Yang, K.R. Ratinac, S.P. Ringer, P. Thordarson, J.J. Gooding, F. Braet, Angew. Chem. Int. Ed. 49 (2010) 2114–2138.
[18] J.F. Rusling, G. Sotzing, F. Papadimitrakopoulosa, Bioelectrochem. 76 (2009) 189–194.
[19] S. Pruneanu, A.R. Biris, F. Pogacean, D.M. Lazar, S. Ardelean, F. Watanabeet al., Chem. Phys. Chem. 13 (2012) 3632–3639.
[20] J.Q. Qian, S.C. Yan, Z.D. Xiao, J. Colloid Interface Sci. 366 (2012) 130–134.
[21] Z.F. Sun, L. Deng, H. Gan, R.J. Shen, M.H. Yang, Y. Zhang, Biosens. Bioelectron. 39 (2013) 215–219.
[22] X.L. Ren, D. Chen, X.W. Meng, F.Q. Tang, A. Du, L. Zhang, Colloid Surf. B-Biointerfaces 72 (2009) 188–192.
[23] W.L. Zhu, Y. Zhou, J.R. Zhang, Talanta 80 (2009) 224–230.
[24] J.J. Zhang, Y.G. Liu, L.P. Jiang, J.J. Zhu, Electrochem. Commun. 10 (2008) 355–358.
[25] D. Du, J. Wang, D.L. Lu, A. Dohnalkova, Y.H. Lin, Anal. Chem. 83 (2011) 6580–6585.
[26] S.C. Yan, X. Xu, Y. Sheng, H.B. Sun, J.S. Wu, L.H. Tang, J. Nanosci. Nanotechnol. 11 (2011) 10320–10323.
[27] Y. Zhang, R. Yuan, Y.Q. Chai, X. Zhong, H.A. Zhong, Surf. Interface Anal. 44 (2012) 1233–1237.
[28] W.S. Hummers, R.E. Offeman, J. Am. Chem. Soc. 80 (1958) 1339–1339.
[29] B. Nikoobakht, M.A. El-Sayed, Chem. Mater. 15 (2003) 1957–1962.
[30] X. Zhao, Y. Liu, J. Lu, J. Zhou, J. Li, Chem. Eur. J. 18 (2012) 3687–3694.
[31] K.C. Lin, Y.C. Lin, S.M. Chen, Analyst 137 (2012) 186–194.
[32] D.A.C. Brownson, J.P. Metters, D.K. Kampouris, C.E. Banks, Electroanalysis 23 (2011) 894–899.
[33] D.W. Pan, W.J. Lu, S.J. Wu, H.Y. Zhang, W. Qin, Mater. Lett. 89 (2012) 333–335.
[34] L. Bai, D. Wen, J.Y. Yin, L. Deng, C.Z. Zhu, S.J. Dong, Talanta 91 (2012) 110–115.
[35] S.D. Yang, C.M. Shen, X.J. Lu, H. Tong, J.J. Zhu, X.G. Zhanget al., Electrochim. Acta 62 (2012) 242–249.
[36] S. Prasannakumar, R. Manjunatha, C. Nethravathi, G.S. Suresh, M. Rajamathi, T.V. Venkatesha, J. Solid State Electrochem. 16 (2012) 3189–3199.
[37] Y. Fan, X. Yang, C.P. Yang, J.H. Liu, Electroanalysis 24 (2012) 1334–1339.
[38] K. Guo, K. Qian, S. Zhang, J.L. Kong, C.Z. Yu, B.H. Liu, Talanta 85 (2011) 1174–1179.
[39] T. Hoshino, H. Muguruma, IEICE Trans. Electron. E95C (2012) 1300–1303.
[40] J.K. Park, H.J. Yee, K.S. Lee, W.Y. Lee, M.C. Shin, T.H. Kimet al., Anal. Chim. Acta 390 (1999) 83–91.
[41] B. Kowalewska, P.J. Kulesza, Anal. Chem. 84 (2012) 9564–9571.
[42] A.M. Pisoschi, A. Pop, A.I. Serban, G.P. Negulescu, J. Electroanal. Chem. 671 (2012) 85–91.